Crab crossing in inverse Compton scattering

A. P. Potylitsyn,[1,2] D. V. Gavrilenko,[2] M. N. Strikhanov,[2] and A. A. Tishchenko[2,3,*]

[1]*National Research Tomsk Polytechnic University, Tomsk 634050, Russian Federation*
[2]*National Research Nuclear University "MEPhI", Moscow 115409, Russian Federation*
[3]*National Research University "BelSU", Belgorod 308034, Russian Federation*

(Received 24 September 2022; accepted 6 March 2023; published 4 April 2023)

Inverse Compton scattering is a promising x-ray source, very bright, quasi-monochromatic, and compact. In this paper, we present a generalized theory of Compton backscattering in terms of luminosity, suitable for both classical and quantum regimes. We show that the optimal parameters, which require a certain mutual orientation and inclination of the fronts of the laser and electron beams described by 3D Gaussians, correspond to the crab scheme. This scheme is widely used in particle physics but is not yet used for x-ray sources. The constructed theory not only predicts the optimal geometry for laser and electron beams but also describes the luminosity. Our results reveal the opportunity to sharply increase the luminosity of compact x-ray sources based on Compton/Thomson backscattering.

DOI: 10.1103/PhysRevAccelBeams.26.040701

I. INTRODUCTION

Inverse Compton scattering from relativistic electrons is one of the most prospective ways to generate quasi-monochromatic x-ray beams [1–9]. It occurs when photons of a laser pulse are scattered on relativistic electrons so that the maximal energy of scattered photons is proportional to the squared Lorentz factor.

To obtain a high-intensity x-ray beam, the most simple and direct way is not to increase the laser power (this leads to a decrease in the monochromaticity of the x-ray beam in a nonlinear regime), but to tilt the fronts of electron and laser beams so that they interact for the longest time. This requires the beams to be oriented along the approach velocity, see Fig. 1. This idea was proposed by Palmer in 1988 [10] for linear colliders and called the "crab-crossing scheme"; then it was developed for ring-shaped machines [11], and now is generally accepted in almost all large accelerator/colliding facilities under the kindred names "crab cavity, crab waist scheme": the world record in luminosity in the particle physics at KEKB.

High Luminosity LHC [12] means tenfold times increasing of luminosity in 2029; proton-proton stage for Future Circular Collider, positron-electron collider [13], future Electron-Ion Collider being constructed jointly by Jefferson Lab and BNL [14], etc.—they all are based on crab crossing [15,16].

In terms of inverse Compton scattering, the first steps in the direction of the realization of the crab-crossing scheme were made in the papers [17,18]. In [17], Bulyak and Skomorokhov, using the luminosity representation, showed that the maximal yield of scattered photons takes place for a head-on collision of the electron and laser beams. The theory constructed in terms of luminosity is attractive as it allows one to take into account the effects of not only classical but also quantum electrodynamics, including nonlinear effects in strong laser fields, etc. Yet, as the authors of [17] indicated, in the Compton sources, the head-on collision is not acceptable for technological reasons. In [18], Variola *et al.* elaborated the theory of [17] considering the tilted electron beam to realize the crab-crossing scheme. In [18], however, they did not consider the tilt of the laser beam front, while, as one can see in Fig. 1, or from the pioneer paper of Palmer [10], in ideal, the true crab-crossing scheme requires both beams to be tilted.

In this study, we have generalized the theory developed in [17,18]. Having accounted for the arbitrary angle of crossing the electron and photon pulses and arbitrary orientations of their fronts, we derive the closed analytical expressions describing the luminosity. In Sec. IV, we show that the influence of nonzero tilt of the laser front is vital for the realization of optimal conditions that prove to coincide with the crab-crossing scheme.

II. COLLISION OF ELECTRON AND PHOTON BEAMS WITH DIRECT FRONTS

In quantum electrodynamics, the process of inverse Compton scattering is described in a more universal way than in classical electrodynamics, based on the cross

*tishchenko@mephi.ru

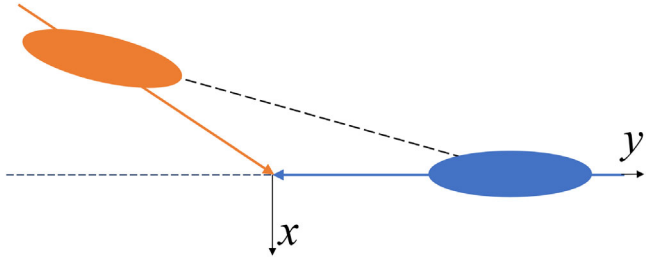

FIG. 1. An optimal geometry—crab-crossing scheme: two colliding beams are oriented along the velocity of approach (dashed line).

section and the luminosity of the process [19]. Using the normalized 3D distribution $F_L(x,y,z)$ of photons in a laser pulse, and introducing the analogous distribution for electron bunch $F_e(x,y,z)$, one obtains the number of scattered photons N_{ph}:

$$N_{ph} = N_L N_e \sigma L,$$
$$L = c(1+\beta\cos\varphi)\int dxdydzdtF_L(x,y-ct,z) \times F_e(x,y+\beta ct,z), \quad (1)$$

where N_L and N_e are the total numbers of particles in the photon pulse and the electron bunch, L—the luminosity, σ—the total cross section of the inverse Compton scattering process, βc—the speed of the electron bunch, $c(1+\beta\cos\varphi)$ is the relative speed of approach of the beams (Fig. 2).

The distribution of laser photons in a form of the production of three Gaussians is defined in the laboratory coordinate system rotated by an angle φ with respect to the dashed one:

$$F_L(x,y,z,t) = \frac{1}{(2\pi)^{3/2}\sigma_{Lx}\sigma_{Ly}\sigma_{Lz}}\exp\left\{-\frac{1}{2}\left[\left(\frac{x'}{\sigma_{Lx}}\right)^2 + \left(\frac{y'-ct}{\sigma_{Ly}}\right)^2 + \left(\frac{z'}{\sigma_{Lz}}\right)^2\right]\right\}, \quad (2)$$

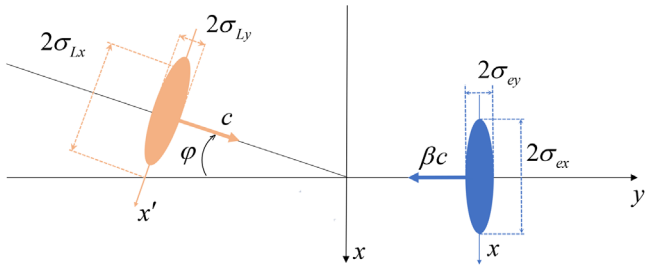

FIG. 2. The layout of the process of inverse Compton scattering; both photon (left, orange) and electron beams (right, blue) have direct fronts: the fronts are perpendicular to the trajectories.

where the dashed coordinates, corresponding to the system rotated by an angle φ:

$$x' = x\cos\varphi - y\sin\varphi,$$
$$y' = x\sin\varphi + y\cos\varphi,$$
$$z' = z. \quad (3)$$

After the substitution of Eq. (3) into Eq. (2), in the approximation $\beta = 1$, the luminosity is calculated as

$$L_\varphi = \left\{2\pi\sqrt{\sigma_{ez}^2+\sigma_{Lz}^2} \times \sqrt{\sigma_{ex}^2+\sigma_{Lx}^2+(\sigma_{ey}^2+\sigma_{Ly}^2)\tan^2(\varphi/2)}\right\}^{-1}. \quad (4)$$

Note that Eq. (4) equals zero at $\varphi = \pi$. Therefore, the sharp increase in the luminosity for $\varphi \to \pi$ shown in Fig. 3 of [17] appears to be incorrect. The general result obtained in Sec. III confirms this conclusion, see Eq. (16) below.

III. COLLISION OF INCLINED ELECTRON AND PHOTON BEAMS WITH TILTED FRONTS (CRAB-CROSSING GEOMETRY)

For geometry shown in Fig. 3, the characteristics of scattered photons will depend on three angular variables: the angles of inclination for each of the beams (ξ for the laser pulse and θ for the electron beam) and the angle of noncollinearity φ—the angle between trajectories. To build the theory that will let us consider the crab-crossing geometry, we have to consider the collision of inclined beams (arbitrary φ) having tilted fronts (arbitrary ξ, θ).

Considering the noncollinear geometry of collision (Fig. 2), Bulyak and Skomorokhov suggested the method that simplifies considerably calculation of luminosity [17]. Following them, we will use 3D Gaussian in the coordinate frame x'', y''

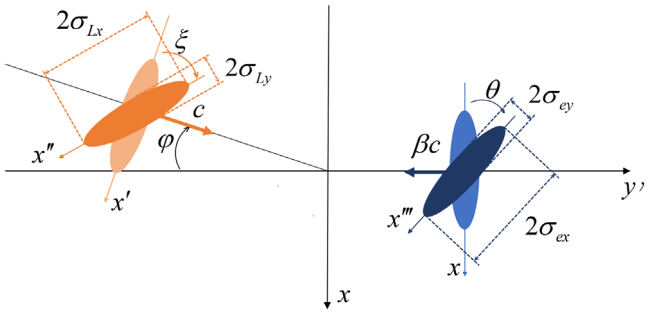

FIG. 3. The layout of the process of inverse Compton scattering; both photon (left, orange) and electron beams (right, blue) have tilted fronts.

$$x'' = x' \cos\xi - y' \sin\xi,$$
$$y'' = x' \sin\xi + y' \cos\xi,$$
$$z'' = z' \tag{5}$$

to describe the laser pulse with the front tilted under the angle ξ with respect to the direction of propagation of the pulse. After the substitution of Eq. (5) into the initial 3D distribution, it is necessary to replace $y' \to y' - ct$ as in Eq. (2) and only after that to pass on to the nondashed coordinates with respect to Eq. (3).

By analogy, to consider the distribution of electrons in the electron beam with front tilted under the angle θ (Fig. 3), we use the replacement

$$x''' = x \cos\theta - (y + \beta ct) \sin\theta,$$
$$y''' = x \sin\theta + (y + \beta ct) \cos\theta,$$
$$z''' = z. \tag{6}$$

After all the substitutions into Eq. (1), the argument of the exponent in the integrand will be a quadratic form in all four variables. For simplicity, replacing the variables

$$x, y, z, ct \to x_1, x_2, x_3, x_4, \tag{7}$$

we write down this exponent as

$$\exp\left\{-\frac{1}{2}\left(\sum_{i,j}^{4} a_{ij} x_i x_j\right)\right\}. \tag{8}$$

Cumbersome calculations allow one to obtain the coefficients a_{ij} in Eq. (8) depending on three angles and six parameters of the Gaussians as elements of the symmetrical matrix:

$$a_{11} = \frac{\cos^2(\theta)}{\sigma_{ex}^2} + \frac{\sin^2(\theta)}{\sigma_{ey}^2} + \frac{\cos^2(\xi+\varphi)}{\sigma_{Lx}^2} + \frac{\sin^2(\xi+\varphi)}{\sigma_{Ly}^2}$$
$$a_{22} = \frac{\sin^2(\theta)}{\sigma_{ex}^2} + \frac{\cos^2(\theta)}{\sigma_{ey}^2} + \frac{\sin^2(\xi+\varphi)}{\sigma_{Lx}^2} + \frac{\cos^2(\xi+\varphi)}{\sigma_{Ly}^2}$$
$$a_{33} = \frac{1}{\sigma_{ez}^2} + \frac{1}{\sigma_{Lz}^2}$$
$$a_{44} = \frac{1}{2}\left(\frac{\beta^2}{\sigma_{ex}^2} + \frac{\beta^2}{\sigma_{ey}^2} + \frac{1}{\sigma_{Lx}^2} + \frac{1}{\sigma_{Ly}^2} + \beta^2\left(\frac{1}{\sigma_{ey}^2} - \frac{1}{\sigma_{ex}^2}\right)\cos(2\theta) + \left(\frac{1}{\sigma_{Ly}^2} - \frac{1}{\sigma_{Lx}^2}\right)\cos(2\xi)\right)$$
$$a_{12} = \frac{1}{2}\left(\left(\frac{1}{\sigma_{ex}^2} - \frac{1}{\sigma_{ey}^2}\right)\sin(2\theta) + \left(\frac{1}{\sigma_{Lx}^2} - \frac{1}{\sigma_{Ly}^2}\right)\sin[2(\xi+\varphi)]\right)$$
$$a_{14} = \frac{1}{2}\left(\beta\left(\frac{1}{\sigma_{ey}^2} - \frac{1}{\sigma_{ex}^2}\right)\sin(2\theta) - \left(\frac{1}{\sigma_{Ly}^2} + \frac{1}{\sigma_{Lx}^2}\right)\sin(\varphi) + \left(\frac{1}{\sigma_{Lx}^2} - \frac{1}{\sigma_{Ly}^2}\right)\sin(2\xi+\varphi)\right)$$
$$a_{24} = \frac{1}{2}\left(-\beta\left(\frac{1}{\sigma_{ex}^2} - \frac{1}{\sigma_{ey}^2}\right) + \beta\left(\frac{1}{\sigma_{ex}^2} - \frac{1}{\sigma_{ey}^2}\right)\cos(2\theta) + \left(\frac{1}{\sigma_{Lx}^2} + \frac{1}{\sigma_{Ly}^2}\right)\cos(\varphi) + \left(\frac{1}{\sigma_{Ly}^2} - \frac{1}{\sigma_{Lx}^2}\right)\cos(2\xi+\varphi)\right); \tag{9}$$

The rest coefficients are zero. For a direct (untilted, $\xi = 0$) electron beam and laser beam having a tilted front (θ is arbitrary), the coefficients a_{ij} from Eq. (9) coincide exactly with those from the paper [18].

When the matrix $\hat{a}$ is reduced to a diagonal form, the exponent in Eq. (8) is written as

$$\exp\left\{-\frac{1}{2}\left(\sum_{i=1}^{4} A_i \eta_i^2\right)\right\}. \tag{10}$$

Calculating the luminosity and using the replacement $\{x_i\} \to \{\eta_i\}$ with a unit Jacobian of the transition, instead of a fourfold integral, it is required to calculate the production of four single integrals:

$$L = \frac{1}{(2\pi)^3} \frac{1+\cos\varphi}{\sigma_{ex}\sigma_{ey}\sigma_{ez}\sigma_{Lx}\sigma_{Ly}\sigma_{Lz}} \prod_{i=1}^{4} \int d\eta_i \exp\left(-\frac{A_i}{2}\eta_i^2\right). \tag{11}$$

Having performed the elementary integrating (the limits of change of the variables η_i rest infinite), we obtain

$$L = \frac{1}{2\pi} \frac{1+\cos\varphi}{\sigma_{ex}\sigma_{ey}\sigma_{ez}\sigma_{Lx}\sigma_{Ly}\sigma_{Lz}} \frac{1}{\sqrt{\det A}}. \tag{12}$$

Thus, the main obstacle here is the calculation of the determinant in the denominator. Having used the equality $\det A = \det a$, we obtain

$$\det A = \left(\frac{1}{\sigma_{ez}^2}+\frac{1}{\sigma_{Lz}^2}\right)\times\left\{\frac{[\beta\cos\theta+\cos(\varphi-\theta)]^2}{\sigma_{ey}^2\sigma_{Lx}^2\sigma_{Ly}^2}+\frac{[\beta\sin\theta-\sin(\varphi-\theta)]^2}{\sigma_{ey}^2\sigma_{Lx}^2\sigma_{Ly}^2}+\frac{[\cos\xi+\beta\cos(\varphi+\xi)]^2}{\sigma_{ey}^2\sigma_{Lx}^2\sigma_{Ly}^2}+\frac{[\sin(\xi)+\beta\sin(\varphi+\xi)]^2}{\sigma_{ey}^2\sigma_{Lx}^2\sigma_{Ly}^2}\right\}. \quad (13)$$

Following the designations from [18], one can present the luminosity in Eq. (12) as

$$L(\varphi,\theta,\xi) = \frac{1}{2\pi\sqrt{\sigma_{ez}^2+\sigma_{Lz}^2}\sqrt{f_e(\varphi,\theta)+f_L(\varphi,\xi)}}, \quad (14)$$

$$f_e(\varphi,\theta) = \sigma_{ex}^2\left[\frac{\beta\cos\theta+\cos(\varphi-\theta)}{1+\beta\cos\varphi}\right]^2+\sigma_{ey}^2\left[\frac{\beta\sin\theta-\sin(\varphi-\theta)}{1+\beta\cos\varphi}\right]^2, \quad (15)$$

$$f_L(\varphi,\xi) = \sigma_{Lx}^2\left[\frac{\cos\xi+\beta\cos(\varphi+\xi)}{1+\beta\cos\varphi}\right]^2+\sigma_{Ly}^2\left[\frac{\sin(\xi)+\beta\sin(\varphi+\xi)}{1+\beta\cos\varphi}\right]^2. \quad (16)$$

The function $f_e(\varphi,\theta)$ characterizing the inclined electron bunch coincides with that from [18] (see Eq. (11a) in [18]). Equation (14) transforms into Eq. (10) from [18] at $\xi = 0$ (in [18] only case, $\xi = 0$ was considered).

Note that Eqs. (15) and (16) depend on the inclination angles ξ and θ the same way (up to the direction), as one would expect. Moreover, each of Eqs. (15) and (16) is invariant relatively to the simultaneous replacement ($\sigma_{ey}\leftrightarrow\sigma_{ex}$,$\sigma_{Ly}\leftrightarrow\sigma_{Lx}$) and ($\theta\leftrightarrow\theta+\pi/2$, $\xi\leftrightarrow\xi+\pi/2$). Indeed, the first pair of replacements change the axes, while the second one returns them with the corresponding rotation.

IV. RESULTS AND DISCUSSION

To define the optimal angles corresponding to the maximal luminosity, one has to differentiate Eq. (15):

$$\frac{\partial f_e}{\partial\theta} = \frac{2}{(1+\beta\cos\varphi)^2}(\sigma_{ex}^2-\sigma_{ey}^2)\Phi_e(\varphi,\theta)\Psi_e(\varphi,\theta)$$
$$\frac{\partial^2 f_e}{\partial\theta^2} = \frac{2}{(1+\beta\cos\varphi)^2}(\sigma_{ex}^2-\sigma_{ey}^2)\{\Psi_e^2(\varphi,\theta)-\Phi_e^2(\varphi,\theta)\} \quad (17)$$

$$\Phi_e(\varphi,\theta) = \beta\cos\theta+\cos(\varphi-\theta)$$
$$\Psi_e(\varphi,\theta) = -\beta\sin\theta+\sin(\varphi-\theta) \quad (18)$$

Similarly, from Eq. (16), one obtains

$$\frac{\partial f_L}{\partial\xi} = \frac{2}{(1+\beta\cos\varphi)^2}(\sigma_{Ly}^2-\sigma_{Lx}^2)\Phi_L(\varphi,-\xi)\Psi_L(\varphi,-\xi)$$
$$\frac{\partial^2 f_L}{\partial\xi^2} = \frac{2}{(1+\beta\cos\varphi)^2}(\sigma_{Lx}^2-\sigma_{Ly}^2)\times\{\Psi_L^2(\varphi,-\xi)-\Phi_L^2(\varphi,-\xi)\}$$
$$\Phi_L(\varphi,\xi) = \cos\xi+\beta\times\cos(\varphi-\xi),$$
$$\Psi_L(\varphi,\xi) = -\sin\xi+\beta\sin(\varphi-\xi). \quad (19)$$

Thus, Eq. (14) is maximal when

$$\sigma_{ey}^2>\sigma_{ex}^2\Rightarrow\tan\theta_{\text{optimal}} = \frac{\sin\varphi}{\beta+\cos\varphi}, \qquad \tan\xi_{\text{optimal}} = -\frac{\sin\varphi}{\beta^{-1}+\cos\varphi},$$
$$\sigma_{ey}^2<\sigma_{ex}^2\Rightarrow\tan\theta_{\text{optimal}} = -\frac{\beta+\cos\varphi}{\sin\varphi}, \qquad \tan\xi_{\text{optimal}} = \frac{\beta^{-1}+\cos\varphi}{\sin\varphi}. \quad (20)$$

Note that Eq. (20) defines the optimal angles θ_{optimal} and ξ_{optimal} at which the luminosity is maximal; and although these optimal angles do not depend on the beam's sizes, the optimalor maximal luminosity does, see Eq. (14).

Within the approximation $\beta = 1$, Eq. (20) reads

$$\sigma_{ey}^2>\sigma_{ex}^2\Rightarrow\theta_{\text{optimal}} = \varphi/2, \qquad \xi_{\text{optimal}} = -\varphi/2,$$
$$\sigma_{ey}^2<\sigma_{ex}^2\Rightarrow\theta_{\text{optimal}} = \varphi/2+\pi/2, \qquad \xi_{\text{optimal}} = -\varphi/2+\pi/2. \quad (21)$$

Of these conditions, the condition $\xi_{\text{optimal}} = -\frac{\varphi}{2}$ was obtained in [1] from geometrical optics by Debus *et al.*, who were the first to propose the idea of using a laser pulse with a tilted front to increase the effective length of interaction between electrons and photons (the size of the electron beam was neglected, and hence the angle θ was not involved); the condition $\theta_{\text{optimal}} = \varphi/2$ was obtained in [18] in terms of luminosity representation.

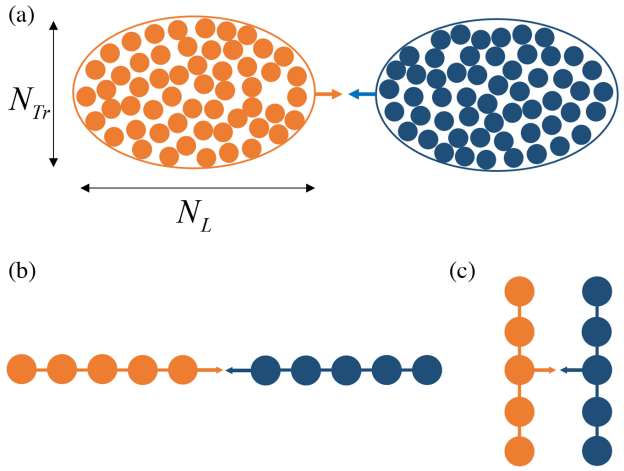

FIG. 4. Collision of the beams of different shapes: (a) general case (the beams have finite thickness and length), (b) elongated beams (each particle interacts with each: N^2 collisions), (c) short beams (each particle interacts with another: N collisions). For simplicity, the beams are depicted as having identical forms or sizes.

The reason why Eq. (21) contains two conditions different for the beams of different forms is understandable: the luminosity is maximal when the beams go through each other being parallel to the direction along their "elongation" (see Fig. 4 and also Fig. 1), and a change in the beam shapes can lead to a rotation of this direction up to $\pi/2$. Thus, the maxima of elongated beams correspond to the minima of the short beams and vice versa. As the elongated beams are optimal, below we will consider this very case.

In Figs. 4(b) and 4(c), we demonstrate that when two chains containing N particles each (the limiting case of elongated beams) collide, the effective number of colliding particles depends on the orientation of the chains: N^2 if they are parallel to the velocity [Fig. 4(b)], and N if they are perpendicular [Fig. 4(c)]. Thus, in general case, when the number of particles in longitudinal and transversal directions is N_L and N_{Tr} correspondingly, then the effective number of particles' collisions is $N_L^2 N_{\mathrm{Tr}}$. Therefore, in general case, it is advantageous for the elongated beams to be oriented along the approach velocity, which coincides with the crab-crossing scheme, see Fig. 1.

Note that a simple overlap of two beams in the collision point is not sufficient: the key factor here is that both beams while overlapping move along the directions of their elongation. For example, both situations in Figs. 4(b) and 4(c) imply a complete overlap of two beams, but only Fig. 4(b) provides the optimal conditions of crab crossing. It is evident therefore that the attempt to realize the crab-crossing scheme undertaken in [18] without nonzero angle ξ could not lead to the optimal conditions; below we will see what role the angle ξ plays.

Now let us analyze the dependence of the luminosity from Eq. (14) on the characteristics of the laser pulse, neglecting the dependence on the size of the electron beam ($\sigma_e \to 0$). For simplicity, we consider the symmetric form of the laser pulse, i.e., $\sigma_{Lx} = \sigma_{Lz} = \sigma_L$. Then Eq. (14) reads

$$L(\varphi, 0) = \frac{1}{2\pi\sigma_L^2 \sqrt{1 + (\sigma_{Ly}/\sigma_L)^2 \left(\frac{\sin\varphi}{1+\cos\varphi}\right)^2}}. \quad (22)$$

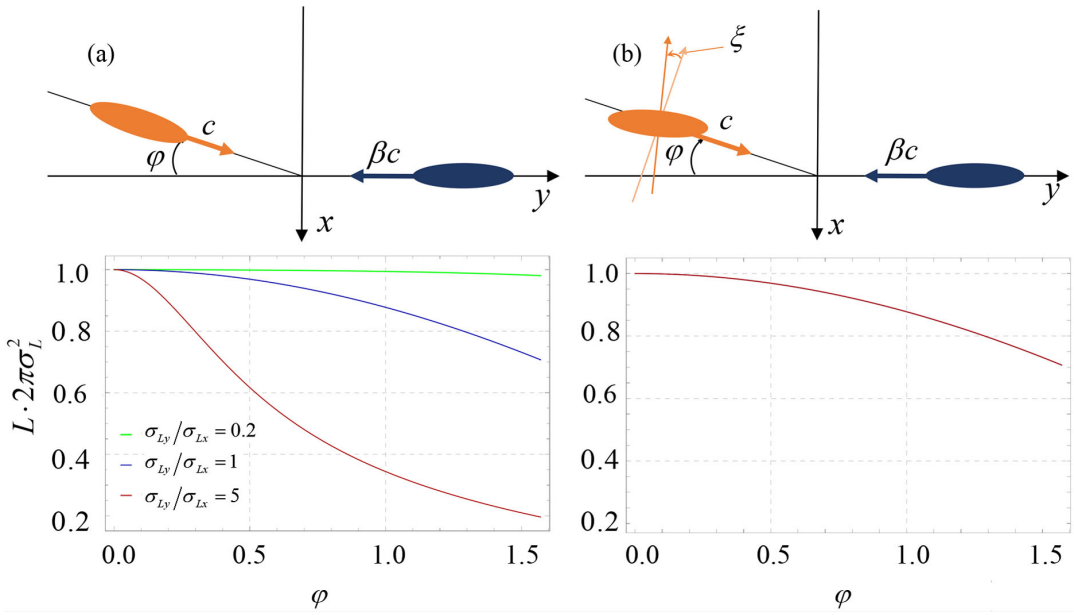

FIG. 5. Dependence of the luminosity on the noncollinearity angle φ for in the case of scattering of the laser pulse on the electron bunch with negligible sizes ($\sigma_e \to 0$) for various lengths of the pulse σ_{Ly}: (a)—left—the laser pulse has perpendicular front ($\xi = 0$), (b)—right—the front of the laser pulse is tilted, $\xi = -\varphi/2$ (optimal angle ξ).

In Fig. 5(a), we show the dependences of the luminosity on the noncollinearity angle φ for the standard pulse with perpendicular front ($\xi = 0$) for various lengths of the pulse σ_{Ly}.

As follows from Fig. 5(a), for a short laser pulse, noncollinearity ($\varphi \neq 0$) practically does not reduce the luminosity compared with the head-on collision ($\varphi = 0$). On the other hand, with increasing the pulse length, in the case of $\sigma_{Ly} > \sigma_L$, noncollinearity leads to the significant suppression of the luminosity.

Yet, for the laser pulse with a front tilted at the angle $\xi = -\varphi/2$, the luminosity does not depend on the pulse length and is defined by the transverse size only, see Fig. 5(b):

$$L_1(\varphi, \xi = -\varphi/2) = \frac{\cos(\varphi/2)}{2\pi\sigma_L^2}. \tag{23}$$

Naturally, for a spherically symmetric pulse $\sigma_{Ly} = \sigma_L$, the luminosity does not depend on the angle ξ.

For a long laser pulse ($\sigma_{Ly}/\sigma_L = 5$), the luminosity has a maximum if $\xi = -\varphi/2$ (see Fig. 6). The authors of [18] considered the laser beam with a perpendicular front $\xi = 0$; the luminosity, in this case, is maximal only at $\varphi = 0$, otherwise it is reduced, see Figs. 5 and 6.

Let us consider the geometry when both beams, electron and photon, have tilted fronts. To analyze the influence of the sizes of both tilted beams on the luminosity, we consider the ratio called the geometric factor in [18]:

$$G(\phi, \theta, \xi) = L(\phi, \theta, \xi)/L(0, 0, 0) \tag{24}$$

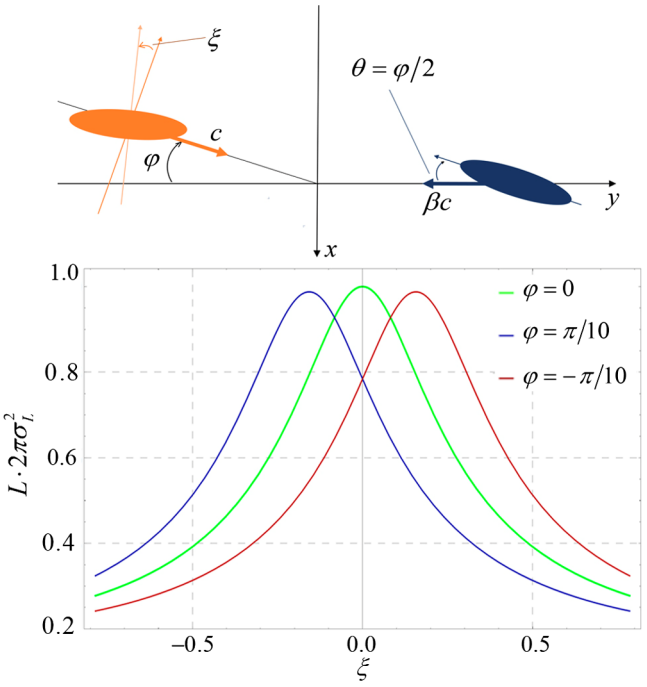

FIG. 6. The luminosity depending on the angle of tilt ξ of the front of a laser pulse for the long pulse ($\sigma_{Ly}/\sigma_L = 5$).

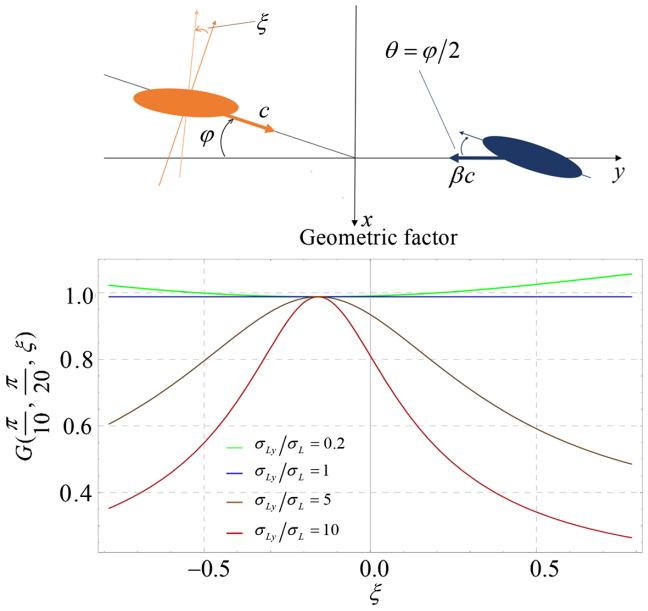

FIG. 7. Geometric factor $G(\pi/10, \pi/20, \xi)$ depending on the inclination angle of the laser pulse ξ for various ratios of its longitudinal and transversal sizes when colliding with an inclined electron bunch.

In Fig. 7, the geometric factor $G(\pi/10, \pi/20, \xi)$ as a function of the angle ξ is shown for noncollinear collision at $\varphi = \pi/10$ and $\theta = \pi/20$. As follows from the figure, there is a maximum at $\xi = -\varphi/2$.

Note that results of [18], being obtained for the case of untilted laser fronts only, correspond to the vertical line $\xi = 0$ in ξ-dependences in Figs. 6 and 7. We see that the accounting for the nonzero angle ξ is of primary importance for reaching a maximum radiation intensity.

VI. CONCLUSION

In this paper, we described colliding bunches by three-dimensional Gaussians, which is more realistic than the classical approach [1,2]. To consider the parameters of colliding bunches in the next approximation depending on the Rayleigh length for the laser and on the beta function for the electron beam, it is necessary to simulate numerically the process of inverse Compton scattering [4,6,20]. Yet, the general theory developed above for an arbitrary geometry, including all conceivable angles of mutual orientation and inclination of the fronts of the laser and electron beams, predicts the optimal geometry, expressed by Eq. (20) (which corresponds to the crab-crossing scheme well known in particle physics), and gives analytical formulas for the luminosity and the number of scattered photons based on Eqs. (14)–(16), which are applicable in a wide range of parameters, both within the frames of classical electrodynamics (moderate laser fields and linear effects) and quantum electrodynamics (intense laser fields and nonlinear effects).

On the other hand, the theory developed above is based on the description of the process in terms of luminosity. Using Eq. (1) only gives the total number of scattered photons and does not provide any information about the energy spectrum, divergence, and energy-angle correlation of scattered photons. The spectral and angular distributions of radiated or scattered photons, however, are possible to obtain using a differential cross section instead of the integral one in Eq. (1), see, e.g., [21]. Yet the quick evaluation of the integral number of scattered photons as a function of parameters of colliding beams is useful to design Compton sources.

Allowing for the possibility of mutual rotation of laser and electron pulses is the key to implementing the crab scheme. As in particle and accelerator physics, this scheme leads to a sharp increase in luminosity, we may hope that the theory developed above can pave the way for a more efficient x-ray source based on inverse Compton scattering.

ACKNOWLEDGMENTS

The study is supported by RFBR, Grant No. 19-29-12036 (Sec. III), and by the Ministry of Science and Higher education of the Russian Federation, the agreement No. FZWG-2020-0032 (2019-1569) (Sec. II) and the Contract No. 075-15-2021-1361 (Sec. IV). The contribution from A. P. P. was partly supported by the TPU (Grant No. FSWW-2020-0008).

[1] A. D. Debus, M. Bussmann, M. Siebold, A. Jochmann, U. Schramm, T. E. Cowan, and R. Sauerbrey, Traveling-wave Thomson scattering and optical undulators for high yield EUV and X-ray sources, Appl. Phys. B **100**, 61 (2010).

[2] K. Steiniger, D. Albach, M. Bussmann, M. Loeser, R. Pausch, F. Röser, U. Schramm, M. Siebold, and A. Debus, Building an optical free-electron laser in the traveling-wave Thomson-scattering geometry, Front. Phys. **6**, 155 (2019).

[3] R. Rullhusen, X. Artru, and P. Dhez, *Novel Radiation Sources Using Relativistic Electrons* (World Scientific, Singapore, 1998).

[4] F. V. Hartemann, W. J. Brown, D. J. Gibson, S. G. Anderson, A. M. Tremaine, P. T. Springer, A. J. Wootton, E. P. Hartouni, and C. P. J. Barty, High-energy scaling of Compton scattering light sources, Phys. Rev. ST Accel. Beams **8**, 100702 (2005).

[5] K. Deitrick, G. H. Hoffstaetter, C. Franck, B. D. Muratori, P. H. Williams, G. A. Krafft, B. Terzić, J. Crone, and H. Owen, Intense monochromatic photons above 100 keV from an inverse Compton source, Phys. Rev. Accel. Beams **24**, 050701 (2021).

[6] G. Paternò, P. Cardarelli, M. Bianchini, A. Taibi, I. Drebot, V. Petrillo, and R. Hajima, Generation of primary photons through inverse Compton scattering using a Monte Carlo simulation code, Phys. Rev. Accel. Beams **25**, 084601 (2022).

[7] S. G. Rykovanov, C. G. R. Geddes, C. B. Schroeder, E. Esarey, and W. P. Leemans, Controlling the spectral shape of nonlinear Thomson scattering with proper laser chirping, Phys. Rev. Accel. Beams **19**, 030701 (2016).

[8] M. A. Valialshchikov, V. Yu. Kharin, and S. G. Rykovanov, Narrow Bandwidth Gamma Comb from Nonlinear Compton Scattering Using the Polarization Gating Technique, Phys. Rev. Lett. **126**, 194801 (2021).

[9] A. Gonoskov, T. G. Blackburn, M. Marklund, and S. S. Bulanov, Charged particle motion and radiation in strong electromagnetic fields, Rev. Mod. Phys. **94**, 045001 (2022).

[10] R. B. Palmer, Energy scaling, crab crossing and the pair problem, in *Proceedings of the 4th DPF Summer Study on High-energy Physics in the 1990s* (Snowmass, CO, USA, 1988), pp. 613–619, https://cds.cern.ch/record/194990?ln=en.

[11] K. Oide and K. Yokoya, Beam-beam collision scheme for storage-ring colliders, Phys. Rev. A **40**, 315 (1989).

[12] *The High Luminosity Large Hadron Collider*, edited by O. Brüning and L. Rossi (World Scientific, Singapore, 2015).

[13] W. Xu, J. Fite, D. Holmes, Z. A. Conway, R. A. Rimmer, S. Seberg, K. Smith, and A. Zaltsman, Broadband high power rf window design for the BNL Electron Ion Collider, Phys. Rev. Accel. Beams **25**, 061001 (2022).

[14] M. Zobov, D. Alesini, M. E. Biagini *et al.*, Test of "Crab-Waist" Collisions at the DAΦNE Φ Factory, Phys. Rev. Lett. **104**, 174801 (2010).

[15] Q. Wu, Crab cavities: Past, present, and future of a challenging device, in *Proceedings of IPAC 2015, 3643* (Richmond, VA, USA, 2015), THXB2.

[16] CERN, official website, https://cerncourier.com/a/crab-cavities-enter-next-phase/.

[17] E. Bulyak and V. Skomorokhov, Parameters of Compton x-ray beams: Total yield and pulse duration, Phys. Rev. ST Accel. Beams **8**, 030703 (2005).

[18] A. Variola, F. Zomer, E. Bulyak, P. Gladkikh, V. Skomorokhov, T. Omori, and J. Urakawa, Luminosity optimization schemes in Compton experiments based on Fabry-Perot optical resonators, Phys. Rev. ST Accel. Beams **14**, 031001 (2011).

[19] J. Yang, M. Washio, A. Endo, and T. Hori, Evaluation of femtosecond X-rays produced by Thomson scattering under linear and nonlinear interactions between a low-emittance electron beam and an intense polarized laser light, Nucl. Instrum. Methods Phys. Res., Sect. A **428**, 556 (1999).

[20] V. Petrillo, A. Bacci, R. Ben Alì Zinati, I. Chaikovska, C. Curatolo, M. Ferrario, C. Maroli, C. Ronsivalle, A. R. Rossi, L. Serafini, P. Tomassini, C. Vaccarezza, and A. Variola, Photon flux and spectrum of g-rays Compton sources, Nucl. Instrum. Methods Phys. Res., Sect. A **693**, 109 (2012).

[21] P. Moskal, R. Czyżykiewicz (COSY-11 Collaboration), Luminosity determination for the quasi-free nuclear reactions, *AIP Conf. Proc.* 950, 118 (2007).